Drivers of future seasonal cycle changes of oceanic pCO_2

M. Angeles Gallego[1], Axel Timmermann[2,3,4], Tobias Friedrich[2], and Richard E. Zeebe[1]

[1]Department of Oceanography, School of Ocean and Earth Sciences and Technology, University of Hawaii at Manoa, Honolulu, Hawaii, USA
[2]International Pacific Research Center, School of Ocean and Earth Sciences and Technology, University of Hawaii at Manoa, Honolulu, Hawaii, USA
[3]Center for Climate Physics, Institute for Basic Science (IBS), Busan, South Korea
[4]Pusan National University, Busan, South Korea

Correspondence: Angeles Gallego(mdla@hawaii.edu)

Abstract. Recent observation-based results show that the seasonal amplitude of surface ocean partial pressure of CO_2 (pCO_2) has been increasing on average at a rate of 2-3 μatm per decade (Landschützer et al., 2018). Future increases of pCO_2 seasonality are expected, as marine CO_2 will increase in response to increasing anthropogenic carbon emissions (McNeil and Sasse, 2016). Here we use 7 different global coupled atmosphere/ocean/carbon cycle/ecosystem model simulations, conducted as part of the Coupled Model Intercomparison Project Phase 5 (CMIP5), to study future projections of the pCO_2 annual cycle amplitude and to elucidate the causes of its amplification. We find, that for the RCP8.5 emission scenario the seasonal amplitude (climatological maximum-minus-minimum) of upper ocean pCO_2 will increase by a factor of 1.5 to 3 times over the next 60-80 years. To understand the drivers and mechanisms that control the pCO_2 seasonal amplification we develop a complete analytical Taylor expansion of pCO_2 seasonality in terms of its four drivers: dissolved inorganic carbon (DIC), total alkalinity (TA), temperature (T) and salinity (S). Using this linear approximation we show that the DIC and T terms are the dominant contributors to the total change in pCO_2 seasonality. To first order, their future intensification can be traced back to a doubling of the annual mean pCO_2, which enhances DIC and alters the ocean carbonate chemistry. Regional differences in the projected seasonal cycle amplitude are generated by spatially varying sensitivity terms. The subtropical and equatorial regions (40°S-40°N), will experience a ≈30-80μatm increase in seasonal cycle amplitude almost exclusively due a larger background CO_2 concentration that amplifies the T seasonal effect on solubility. This mechanism is further reinforced by an overall increase in the seasonal cycle of T, as a result of stronger ocean stratification and a projected shoaling of mean mixed layer depths. The Southern Ocean will experience a seasonal cycle amplification of ≈90-120 μatm in response to the mean pCO_2-driven change of the mean DIC contribution and to a lesser extent to the T contribution. However, a decrease of the DIC seasonal cycle amplitude somewhat counteracts this regional amplification mechanism.

1 Introduction

Owing to its large chemical capacity to resist changes in CO_2 concentration ($[CO_2]$) (referred to as buffering capacity), the ocean has absorbed nearly half of the anthropogenic CO_2 produced by fossil fuel burning and cement production since the industrial revolution (Sabine et al., 2004). While the ocean's absorption of CO_2 lowers the atmospheric concentration, it also

increases the ocean's [CO_2] and in turn lowers its buffering capacity. This leads to a reduction in the oceanic uptake of CO_2 and an intensification of the pCO_2 seasonal cycle (from now on referred to as δpCO_2) (McNeil and Sasse, 2016; Völker et al., 2002). In a recent key observational study by Landschützer et al. (2018), it was demonstrated that the δpCO_2 amplitude has increased at a rate of ≈2-3 μatm per decade, from 1982 to 2015.

The pCO_2 already experiences large seasonal fluctuations, which in some regions can reach up to 60% above and below the annual mean pCO_2, (Takahashi et al., 2002). An intensification of the δpCO_2 amplitude could produce seasonal hypercapnia conditions (McNeil and Sasse, 2016) which, together with increased $[H^+]$ seasonality (Kwiatkowski and Orr, 2018; Hagens and Middelburg, 2016) and aragonite undersaturation events (Hauri et al., 2015; Sasse et al., 2015; Shaw et al., 2013) could expose marine life to harmful seawater conditions earlier than expected if considering only annual mean values. Moreover, a projected amplification of δpCO_2 might increase the net CO_2 uptake in some regions, such as the Southern Ocean, thereby further accelerating the decrease of the buffering capacity in that region (Hauck and Völker, 2015).

The pCO_2 seasonal amplitude is controlled mainly by the seasonal changes in temperature (T) and biological activity together with upwelling changes that alter DIC concentrations. Usually, DIC and T changes work in opposite directions (**?**Takahashi et al., 2002; Fay and McKinley, 2017). In subtropical regions higher pCO_2 values occur in summer when solubility decreases. In subpolar regions, pCO_2 increases in winter when waters upwell that are rich in DIC and when respiration of organic matter takes place. Decreased subpolar pCO_2 occurs in summer when the primary productivity is higher and the upwelling diminishes. Therefore, we find close relationships of δpCO_2 with the ocean's $[CO_2]$ that controls the chemical reactions and with the mean pCO_2 that moderates the exchange with the atmosphere. Both factors are related by the solubility constant that depends on temperature and salinity.

Furthermore, the regional differences in the influence of temperature and biology on δpCO_2 are modulated by the ocean's buffering capacity. This is due to the ability of CO_2 to react with seawater to form bicarbonate $[HCO_3^-]$ and carbonate $[CO_3^{2-}]$, leaving only a small portion of the dissolved carbon dioxide in the form of aqueous CO_2 ([CO_2(aq)]). [CO_2(aq)] together with the carbonic acid ($[H_2CO_3]$) are defined as [CO_2]. Therefore, it is useful to define the total amount of carbon as DIC, which is the sum of the three carbon species ($[HCO_3^-]$, $[CO_3^{2-}]$ and [CO_2]). At current chemical conditions, most of the DIC is in form of HCO_3^-, therefore the buffering capacity is largely controlled by the CO_3^{2-} capable of transforming CO_2 into bicarbonate through the reaction $CO_2(aq) + CO_3^{2-} + H_2O = 2HCO_3^-$ (Zeebe and Wolf-Gladrow, 2001). The larger the buffering capacity, the larger the pCO_2's ability to resist changes in DIC. To quantify this capacity, we can introduce the sensitivity factor γ_{DIC}, which is inversely related to the buffering capacity, defined as $\gamma_{DIC} = \partial \ln(pCO_2)/\partial DIC$, (Egleston et al., 2010). Other sensitivity factors are related to the total alkalinity (γ_{TA}), salinity (γ_S) and temperature (γ_T) changes, and are defined in a similar way as $\partial \ln(pCO_2)/\partial TA$, $\partial \ln(pCO_2)/\partial S$ and $\partial \ln(pCO_2)/\partial T$ respectively. It is important to note that the pCO_2 is highly sensitive to temperature due to two factors: first through solubility changes that account for 2/3 of the present day temperature impact, and second, through the dissociation constants that control the carbon system reactions (Sarmiento and Gruber, 2006).

While the mechanisms controlling the seasonal cycle of pCO_2 at present day are well documented, the future evolution of these drivers has not been fully elucidated. Current literature suggests that the seasonal amplification is a consequence of an

increase on the T and DIC contributions to δpCO_2 (Landschützer et al., 2018) and an increased sensitivity of the ocean to these variables (Fassbender et al., 2017).

The aim of our paper is to provide an in-depth analysis of the mechanisms controlling the future strength of δpCO_2 and its regional differences using 7 CMIP5 global earth system models. Our analysis focuses on the 21^{st} century evolution using the Representative Concentration Pathway 8.5 (RCP8.5) scenario. We give a comprehensive analysis of the projected evolution of the DIC, TA, T and S contributions to pCO_2 seasonality. To achieve this goal, we derive explicit analytical expressions for pCO_2 sensitivities in terms of γ_{DIC}, γ_{TA}, γ_{T} and γ_{S}, thereby extending previous work done by Egleston et al. (2010).

2 Methodology

2.1 CMIP5 Models

For our analysis, pCO_2, DIC, TA, T and S monthly-mean output variables covering the period from 2006-2100 were obtained from future climate change simulations conducted with 7 fully coupled earth system models that participated in the Coupled Model Intercomparison Project, Phase 5 (CMIP5). The following models were selected based on data availability: CanESM2, CESM1-BGC, GFDL-ESM2M, MPI-ESM-LR, MPI-ESM-MR, HadGEM2-ES and HadGEM2-CC (See supplementary material of Hauri et al. (2015)). For the purpose of this paper, we used the Representative Concentration Pathway 8.5 (RCP8.5) future climate change simulations (IPCC, 2013). The ocean's surface data sets were regrided onto a 1^{o}x1^{o} grid using Climate Data Operators (CDO). The Arctic Ocean and the region poleward of 70^{o}S are removed from the analyses, because observational data for model validation are scarce.

2.2 Analysis of δpCO_2

To elucidate the underlying dynamical, thermodynamical, biological and chemical processes controlling δpCO_2 we calculated a first order Taylor series expansion of δpCO_2 in terms of its four drivers, DIC, TA, T and S. While T and S are controlled only by physics, DIC and TA are controlled by physical, chemical and biological processes. Throughout this paper we use salinity-normalized DIC and TA using a mean salinity of 35 psu. This effectively removes the concentration/dilution fresh water effect, following the procedure of Lovenduski et al. (2007). The salinity normalized variables are referred to as DIC_s and TA_s, corresponding to $DIC \cdot S_0/S$ and $TA \cdot S_0/S$ respectively. The freshwater effect on DIC and TA is now included in the S term, renamed as S_{fw}. For the Taylor series expansion, each variable (X=DIC, TA, T and S) is decomposed into $X = \overline{X} + \delta X$. The term $\overline{X}$ represents the 21 years-long mean and δX denotes the seasonal cycle (calculated as the monthly mean deviation from the 21 years average). The Taylor's expansion is then computed for an initial (2006-2026) and final (2080-2100) periods. We use multi-decade means and eventually multi-model ensemble means to remove effects of interannual variability. The full first-order series expansion is given by:

$$\delta pCO_2 \approx \frac{\partial pCO_2}{\partial DIC}\bigg|_{\overline{TA},\overline{DIC}}^{\overline{T},\overline{S}} \delta DIC_s + \frac{\partial pCO_2}{\partial TA}\bigg|_{\overline{TA},\overline{DIC}}^{\overline{T},\overline{S}} \delta TA_s + \frac{\partial pCO_2}{\partial T}\bigg|_{\overline{TA},\overline{DIC}}^{\overline{T},\overline{S}} \delta T + \frac{\partial pCO_2}{\partial S}\bigg|_{\overline{TA},\overline{DIC}}^{\overline{T},\overline{S}} \delta S_{fw} \quad (1)$$

Each term of the right hand side of Eq. (1) represents the contribution from one of the four drivers of δpCO$_2$.

The analytical expressions for the derivatives (without the salinity normalization) are given by:

$$
\begin{aligned}
\left.\frac{\partial pCO_2}{\partial TA}\right|_{\overline{TA},\overline{DIC}}_{\overline{T},\overline{S}} &= \overline{pCO}_2 \cdot \frac{-\overline{Alk}_c}{\overline{DIC}\cdot\Theta - \overline{Alk}_c^2} \\
\left.\frac{\partial pCO_2}{\partial DIC}\right|_{\overline{TA},\overline{DIC}}_{\overline{T},\overline{S}} &= \overline{pCO}_2 \cdot \frac{\Theta}{\overline{DIC}\cdot\Theta - \overline{Alk}_c^2} \\
\left.\frac{\partial pCO_2}{\partial T}\right|_{\overline{TA},\overline{DIC}}_{\overline{T},\overline{S}} &= \overline{pCO}_2 \cdot \frac{1}{\overline{DIC}\cdot\Theta - \overline{Alk}_c^2}\left[\overline{TA}_c \cdot \left(\frac{\partial Alk_c}{\partial T} + \frac{\partial [B(OH)_4^-]}{\partial T} + \frac{\partial [OH^-]}{\partial T}\right) - \Theta \cdot \frac{\partial (DIC - [CO_2])}{\partial T}\right] - \frac{\overline{pCO}_2 \cdot}{\overline{K_0}(T,S)}\frac{\partial K_0(T,S)}{\partial T} \\
\left.\frac{\partial pCO_2}{\partial S}\right|_{\overline{TA},\overline{DIC}}_{\overline{T},\overline{S}} &= \overline{pCO}_2 \cdot \frac{1}{\overline{DIC}\cdot\Theta - \overline{Alk}_c^2}\left[\overline{Alk}_c \cdot \left(\frac{\partial \overline{Alk}_c}{\partial S} + \frac{\partial [B(OH)_4^-]}{\partial S} + \frac{\partial [OH^-]}{\partial S}\right) - \Theta \cdot \frac{\partial (DIC - [CO_2])}{\partial S}\right] - \frac{\overline{pCO}_2 \cdot}{\overline{K_0}(T,S)}\frac{\partial K_0(T,S)}{\partial S}
\end{aligned}
\tag{2}
$$

where $\Theta = [\mathrm{HCO_3^-}] + 4[\mathrm{CO_3^{2-}}] + \frac{[\mathrm{B(OH)_4^-}][\mathrm{H^+}]}{(\mathrm{k_b}+[\mathrm{H^+}])} + [\mathrm{H^+}] + [\mathrm{OH^-}]$ and $\overline{\mathrm{Alk_c}} = [\mathrm{HCO_3^-}] + 2[\mathrm{CO_3^{2-}}]$. The explicit T and S partial derivatives are given in the Supplementary material (Text S1). The first two derivatives coincide with the results of Egleston et al. (2010) and Hagens and Middelburg (2016), with the exception of the sign of $[OH^-]$ in Egleston et al. (2010) term S. To verify this approach we compared the sum of the Taylor expansion terms with the full simulated range of δpCO$_2$ from the model's output. The Taylor expansion reproduces well the full seasonal cycle amplitude of the original climate model simulations (Supplementary Fig. S1). The analytical expressions for temperature and salinity presented in here are – to our knowledge – the first ones of their kind. Previously the calculation of these terms was based on the approximation given by Takahashi et al. (1993) or on numerical calculations.

To gain more insight into the processes causing the amplification of δpCO$_2$ we introduce a method based on a second Taylor series expansion described below. Eq. (1) can be rewritten using the expressions for the sensitivities γ determined by the relation $\frac{1}{\mathrm{pCO_2}}\frac{\partial \mathrm{pCO_2}}{\partial \mathrm{X}} = \gamma_\mathrm{X}$. These sensitivities have been historically used to represent the percentage of change in pCO$_2$ per unit of DIC, TA, T or S. With this notation, Eq. (1) can be expressed in the following way:

$$
\delta pCO_2 \approx \overline{pCO_2} \cdot \left(\gamma_{DIC}\cdot\delta DIC_s + \gamma_{TA}\cdot\delta TA_s + \gamma_T \cdot \delta T + \gamma_{S_{fw}} \cdot \delta S_{fw}\right) \tag{3}
$$

Each term in Eq.(3) consists of three parts: $\overline{\mathrm{pCO_2}}$, the sensitivity γ_X and the corresponding seasonal cycle δX. To understand which component is the main driver for δpCO$_2$ changes, we perform a second Taylor expansion of the end of the century's δpCO$_2$ around the initial state of the system in 2006-2026.

To maximize mathematical clarity we will introduce some definitions: first, we introduce the symbol Δ to indicate the difference between the period 2080-2100 and 2006-2026. Therefore, the total future change in δpCO$_2$, is now referred to as $\Delta\delta$pCO$_2$. In the same manner, the total change in sensitivities and seasonal cycles are written as $\Delta\gamma_{\mathrm{DIC_s}}, \Delta\gamma_{\mathrm{TA_s}}, \Delta\gamma_\mathrm{T}, \Delta\gamma_{\mathrm{S_{fw}}}$, and $\Delta\delta\mathrm{DIC_s}, \Delta\delta\mathrm{TA_s}, \Delta\delta\mathrm{T}, \Delta\delta\mathrm{S_{fw}}$ respectively. Finally, we introduce the vector $\boldsymbol{X}$ formed by the four variables DIC$_\mathrm{s}$, TA$_\mathrm{s}$,

T and S_{fw}, as: $\{X_0, X_1, X_2, X_3\}$=$\{DIC_s, TA_s, T, S\}$. With this notation, we can write an expansion of Eq.(3) of the final state of the system by 2080-2100 named $\mathbf{X}^f$ around the initial state $\mathbf{X}^i = \{DIC_s{}^i, TA_s{}^i, T^i, S^i_{fw}\}$ by 2006-2026 as:

$$
\begin{aligned}
\Delta\delta pCO_2 \quad = \quad & \Delta\overline{pCO}_2 \sum_{k=0}^{3} \gamma_{X_k}{}^i \cdot \delta X_k{}^i \\
+ \quad & \overline{pCO}_2^i \sum_{k=0}^{3} \Delta\gamma_{X_k} \cdot \delta X_k{}^i \\
+ \quad & \overline{pCO}_2^i \sum_{k=0}^{3} \gamma_{X_k}{}^i \cdot \Delta\delta X_k \\
+ \quad & \Delta\overline{pCO}_2 \sum_{k=0}^{3} \Delta\gamma_{X_k} \cdot \delta X_k{}^i \quad (2^{nd} order \quad terms) \\
+ \quad & \Delta\overline{pCO}_2 \sum_{k=0}^{3} \gamma_{X_k}{}^i \cdot \Delta\delta X_k \\
+ \quad & \overline{pCO}_2^i \sum_{k=0}^{3} \Delta\gamma_{X_k} \cdot \Delta\delta X_k \qquad\qquad , \qquad (4)
\end{aligned}
$$

where the first, second and third terms represent the contributions to $\Delta\delta$pCO$_2$ due to changes in the mean pCO$_2$ ($\Delta\overline{\mathrm{pCO}_2}$), the pCO$_2$ sensitivities ($\Delta\gamma_{X_k}$) and the seasonal cycles ($\Delta\delta X_k$) respectively; the fourth to sixth rows are the second order terms. This method is similar to the one used by Landschützer et al. (2018).

3 Results and discussion

3.1 δpCO$_2$ amplification

Figure 1, (a) shows the ensemble mean δpCO$_2$ amplitude (calculated as climatological maximum-minus-minimum) for the initial period 2006-2026. The values range from ≈98 μatm for the high latitudes (40°S-70°S, 40°N-60°N) to ≈60 μatm between 40°S-40°N. The ensemble mean initial seasonal amplitude range is in good agreement with observational estimates calculated for the reference year 2005 (Takahashi et al., 2014b), and for the 1982-2015 period (Landschützer et al., 2017). The agreement between models and observations is remarkably good in the equatorial regions, but the initial amplitude is slightly overestimated in the mid and high latitudes (see Supplementary Fig. S3).The higher amplitude in models than observations is expected, as the initial period 2006-2026 already experienced an amplification compared to previous years. Moreover, Tjiputra et al. (2014) found that the ocean's pCO$_2$ historical trend is larger in models than observations when it is estimated in large scale areas of the ocean. However, they found that models' pCO$_2$ trends agree with observations when the trends are subsampled to the locations where the observations were taken, and therefore they do a good job reproducing well-known time series. Moreover, differences are expected as Pilcher et al. (2015) suggested that CMIP5 models perform well in reproducing the seasonal cycle timing, but still show considerable errors in reproducing the seasonal amplitude of pCO$_2$ due to differences

in the mechanisms represented in each model, especially in subpolar biomes.

By 2080-2100 the annual cycle amplitude attains values of ≈197 μatm and ≈101 μatm in the high and mid-low latitudes respectively (Fig. 1,(b)). These seasonal variations correspond to 20% and 18% of annual $\overline{\mathrm{pCO_2}}$ for the initial and final periods respectively. Figure 1, (c), shows that the global ocean $\delta\mathrm{pCO_2}$ will intensify by a factor of 1.5 to 3 times for the 2080-2100 period relative to the 2006-2026 reference period. Figure 1, (d), shows the difference in amplitude ($\Delta\delta\mathrm{pCO_2}$); this pattern differs from the ratio, because the ratio overestimates the amplification in areas where the initial amplitude is lower than ≈10 μatm. McNeil and Sasse (2016) used observations and a neural-network-clustering algorithm to project that by year 2100, the $\delta\mathrm{pCO_2}$ amplitude in some regions could be up to ten times larger than it was in year 2000. Our mean amplification factor estimation agrees with the mean threefold amplification found for most of the ocean by McNeil and Sasse (2016). However the high values in this previous study can not be reproduced here - mainly because we consider 21 years average ratios instead of single year ratios, which are strongly affected by interannual variability. Using observations, Landschützer et al. (2018) found an increase of 2.2 μatm per decade, which is smaller than our findings of a total 42 μatm increase by the end of the century between 40°S-40°N, and a global-mean change of 81 μatm on the high latitudes. This difference is again possibly due the higher mean $\mathrm{pCO_2}$ values in models than observations.

The global ocean mean amplification factor of $\delta\mathrm{pCO_2}$ roughly coincides with a doubling of $\overline{\mathrm{pCO_2}}$ (Fig. 2). The direct relationship between these two is explained in section 3.5. Figure 1 (e-h) shows the zonal mean panels of (a-d); In general, towards the end of the century the $\mathrm{pCO_2}$ amplifies more in high latitudes, but so does the standard deviation uncertainty among models. This regional pattern agrees with the observation-based findings of Landschützer et al. (2018) which show that high latitudes have already experienced a larger amplification than mid-low latitudes from 1982 to 2015. Furthermore, the same pattern is projected by CMIP5 models for the seasonal amplification of $[\mathrm{H^+}]$ by the end of the century (Kwiatkowski and Orr, 2018). This is expected from the near-linear relation between $\mathrm{pCO_2}$ and $[\mathrm{H^+}]$. These regional differences in amplification for $\mathrm{pCO_2}$ can be explained in terms of the relative magnitudes and the phases between the DIC, TA, T and S contributions, which are explained in subsequent sections.

3.2 Present and future drivers of $\delta\mathrm{pCO_2}$

To understand the driving factors of $\delta\mathrm{pCO_2}$ and its spatiotemporal differences, we split $\delta\mathrm{pCO_2}$ into the four different contributions from $\mathrm{DIC_s}$, $\mathrm{TA_s}$, T and $\mathrm{S_{fw}}$ for the initial and final periods, following Eq. (1). The results are shown in Fig. 3. For most of the ocean, the ensemble mean estimated contributions from $\mathrm{DIC_s}$ and T to the present-day $\delta\mathrm{pCO_2}$ are in good agreement with the data-based estimates of Takahashi et al. (2014b) and Landschützer et al. (2017), particularly in the equatorial regions (see Supplementary Fig. S3). However our T and DIC contributions are slightly larger in mid and high latitudes, for the same reasons the $\mathrm{pCO_2}$ seasonal amplitude is overestimated (see Section 3.1). Also, differences arise between our DIC_s contribution and the observation-based so called "non-thermal" contribution, because the non-thermal contribution also includes the total alkalinity and salinity effects. Nonetheless, between 40°S-40°N our ensemble mean shows that $\delta\mathrm{pCO_2}$ is dominated by changes in temperature that control $\mathrm{CO_2}$ solubility, which decreases in summer enhancing $\mathrm{pCO_2}$, in agreement with observations. The Southern Ocean is controlled by DIC, that responds to changes in upwelling and phytoplankton blooms. Both mechanisms act

together to decrease (increase) DIC in summer (winter) (Sarmiento and Gruber, 2006).

The models show that the δpCO_2 in the 40°N to 60°N band is controlled by T, which disagrees with the above mentioned observations that show a non-temperature dominance in this band. The difference between models and observations arises from two regions: the North Atlantic basin and the North Western Pacific; specifically near the Oyashio Current, and the outflows from the Okhotsk Seas (see Supplementary Fig. S3). Most models show a T dominance in the North Atlantic basin; only CESM1-BGC and GFDL-ESM2M show a DIC dominance (see Supplementary Fig. S4). The North Atlantic is one of the major sinks of anthropogenic CO_2, however some models fail to estimate its uptake capacity (Goris et al., 2018). Goris et al. (2018) found that models with an efficient carbon sequestration present a DIC-dominated pCO_2 seasonal cycle in the North Atlantic, but models with low anthropogenic uptake show a T dominance in this region. In the North-Western Pacific, Mckinley et al. (2006) found that coarse models are not able to capture the intricate oceanographic features of this area, and therefore the pCO_2 seasonality is not well captured.

Towards the end of the century (Fig. 3, right column), the amplification of δpCO_2 is caused by an increase in the DIC_s and T contributions, and to a lesser extent due to TA_s and S_{fw}. Only in the high latitudes the TA_s contribution reinforces the DIC_s effect. The δDIC_s and δT relative phase and magnitude play an important role in causing regional differences of future δpCO_2. For example, between 40°-60°, we find a lower amplification factor than at 30°-40° in both hemispheres (Fig. 1, (c)), contrary to what we expected from the general observed larger amplification at higher latitudes. In this band of lower amplification, the warm water from subtropical regions meets the nutrient rich water from the subpolar regions, but the DIC_s and T effects are almost 6 months out of phase, and therefore their cancellation is larger than in the 30°-40° latitude band; where for example, in the North Atlantic, there is 9 month phase-difference between both contributions. A clear illustration of this phase effect is found in the Supplementary information (Fig. S5).

In the Southern Ocean there is a shift in the maximum δpCO_2 occurring from August-September to March-April (Fig. 3, last row). This shift is generated because the T contribution gains importance over DIC_s, due to a reduction of δDIC_s magnitude at the same time that δT increases (Fig. 5). In the Equatorial Pacific region (Fig. 5), T dominates over DIC_s but both contributions are small due to their low seasonality. Therefore, this region will experience a low amplification in δpCO_2. In this region some models underestimate the pCO_2 trend (Tjiputra et al., 2014), and therefore the seasonal amplification might be underestimated too. In the following sections we conduct further analysis by decomposing each contribution as the result of three factors: the mean pCO_2 ($\overline{pCO_2}$), the regional pCO_2 sensitivities (γ_{DIC}, γ_{TA}, γ_T and $\gamma_{S_{fw}}$) and the seasonal cycles (δDIC_s, δTA_s, δT and δS_{fw}) as determined in Eq. (3).

3.3 Future pCO_2 sensitivities

The γ_{DIC} and γ_{TA} are projected to increase by the end of the century due to a lower ocean buffering capacity produced by increasing temperature and larger background concentrations of DIC (Fassbender et al., 2017). This agrees with our results shown in Fig. 4, which shows that all regions will experience an increase in γ_{DIC} and γ_{TA}. Lower buffer factors (higher sensitivities factors) are found in regions where DIC and TA have similar values, and they will decrease (increase) as the DIC/TA ratio in the oceans increases (Egleston et al., 2010). The alkalinity sensitivity is negative, as pCO_2 decreases with

increasing alkalinity, but we show here the negative of γ_{TA} for better comparison. γ_{TA} will increase (with negative values) more than the DIC sensitivity. However seasonal changes in open-ocean $\mathrm{TA_s}$ are small, and therefore the total contribution of alkalinity in our analysis is negligible compared to the $\mathrm{DIC_s}$ and T contributions. $\gamma_{\mathrm{S_{fw}}}$ decreases everywhere except in the Western Pacific Warm Pool. In this region $\gamma_{\mathrm{S_{fw}}}$ increases probably due to future changes in precipitation that enhance the fresh-water effect. In Fig. 4, the sensitivities (γ) are expressed as a percentage change of $\mathrm{pCO_2}$ per unit in DIC, TA, T and S respectively. This follows the approach of Takahashi et al. (1993), however in their paper the authors compute the Revelle factor, which is related to γ_{DIC} as $\mathrm{R} = \mathrm{DIC} \cdot \gamma_{\mathrm{DIC}}$. To illustrate the meaning of the sensitivities, we will focus on the subtropical North Pacific in the 15°N-40°N latitudinal band. In this region γ_{DIC} indicates an average 0.6% change in $\mathrm{pCO_2}$ per unit of DIC in 2006-2026. Therefore, for a $\delta\mathrm{DIC_s}$ seasonal cycle amplitude of 40 μmol/kg^{-1} and $\overline{\mathrm{pCO_2}} \approx 400$ μatm, the total $\delta\mathrm{pCO_2}$ amplitude equals 96 μatm. Following the same reasoning, by 2080-2100, γ_{DIC} increases to 0.7% and $\delta\mathrm{DIC_s}$ decreases to 30 μmol/kg^{-1}; therefore, for a $\overline{\mathrm{pCO_2}}$ equal to 800 μatm, the $\delta\mathrm{pCO_2}$ amplitude due to δDIC amounts to 168 μatm.

The temperature sensitivity has been experimentally determined by Takahashi et al. (1993); who found a value of 0.0423, meaning that $\mathrm{pCO_2}$ changes by about 4% for every °C. This value agrees with our global mean ensemble estimate of 0.0428. However, our analytical expression of γ_T shows that this value varies regionally and, by reasons unknown to us, it might decrease in the future to a global mean value of 0.0415, (Fig. 4, row (c), third column). The T sensitivity is larger in colder regions and lower in the warmer tropics; however, colder regions will experience a larger reduction on γ_{T}, which locally prevents a larger amplification of the T contribution to $\delta\mathrm{pCO_2}$. In the next section we show that the T seasonality is projected to increase in high latitudes, strengthening the T contribution.

3.4 Future $\delta\mathrm{DIC_s}$, $\delta\mathrm{TA_s}$, δT and $\delta\mathrm{S_{fw}}$.

Towards the end of the century, the global mean amplitude of $\delta\mathrm{DIC_s}$ is projected to decrease by ≈26-28$\%$ in the high latitudes (Fig.5, (a)), according to all the CMIP5 earth system model simulations used here. In the mid-low latitudinal band there is no agreement between models; while some show an increase others project a decrease in amplitude. As suggested by Landschützer et al. (2018), the larger decrease in the Southern Ocean may be the result of changes in the shallow overturning circulation that prevent $\mathrm{CO_2}$ accumulation in this region. This reduction may be counteracted by the predicted increase in productivity owing to a suppression of light and temperature limitations (Steinacher et al., 2010; Bopp et al., 2013).

According to the CMIP5 models, most of the ocean is projected to experience a slight increase in δT, as shown in Fig. 5, column (b). All models show a slight increase in δT, only one model showed a slightly decrease in the southern region, and two models showed a decrease in the equatorial region during October to December. It is important to note that Fig. 5 shows the seasonal values, with the mean T removed. Therefore, when considering the positive T trends, the absolute summer values show an increase and the absolute winter values a decrease. This agrees with the results of Alexander et al. (2018); who showed that models project a seasonal intensification of T, with larger warm extremes and reduced cold extremes. The authors attributed the T seasonality intensification to an increased oceanic stratification and an overall shoaling of the mixed layer depth, which confines seasonal changes in a reduced volume of water, producing larger changes at the surface. They also showed that the intensification trends are stronger in summer than winter, as the mixed layer depth is shallower in summer. Moreover, ice

covered regions will experience the largest increase in T seasonality due the loss of sea ice, because the ice melting/freezing moderates the surface water temperature seasonality(Carton et al., 2015).

The TA seasonality is also projected to increase in the high latitudes according to all models, except CESM1-BGC which shows a decrease. For δS (see Supplementary Fig. S6) there is no agreement among the different CMIP5 models, except in the Southern Ocean where all the models show a slightly decrease. Kwiatkowski and Orr (2018) demonstrated that the seasonality of the drivers is important to determine future changes in $[H^+]$ seasonality. In the same fashion, our results show that the four δpCO_2 drivers present changes in seasonality, and in particular δDIC_s and δT changes are important to explain future projections of the δpCO_2 amplitude. The increase in δT enhances the δpCO_2 amplification, and the reduction of δDIC_s in the Southern Ocean locally prevents a larger amplification.

3.5 Regional dominant factors

To identify the main cause of the $\delta \mathrm{pCO_2}$ amplification we use the Taylor series expansion method. With this method we consider the system's final state (δpCO_2 by 2080-2100) as a perturbation of the initial state (δpCO_2 by 2006-2026), as shown in Eq. (4). The expansion is done in three groups of variables: the seasonal cycles of DIC_s, TA_s, T and S (δX) , the sensitivities of pCO_2 to the same four variables (γ_x), and the mean pCO_2 ($\overline{\mathrm{pCO_2}}$). Therefore, each term of the expansion represents how much of the total δpCO_2 change (indicated by $\Delta\delta \mathrm{pCO_2}$ and calculated as 2080-2100 value- minus-2006-2026 value) is due the change in each of these factors. We also add the second order terms that come from their combination. The results are shown in Fig. 6, (a) and they indicate that the leading cause of the δpCO_2 amplification is the change in $\overline{\mathrm{pCO_2}}$ ($\Delta\overline{\mathrm{pCO_2}}$), which confirms previous findings by Landschützer et al. (2018).

It is important to note that our linear Taylor's expansion approach neglects one aspect of the highly non linear carbonante chemistry of the ocean: it assumes $\overline{\mathrm{pCO_2}}$ and the sensitivities as independent variables, and therefore does not include the positive feedback between larger $\overline{\mathrm{pCO_2}}$ and increasing γ_{DIC} (decreasing buffering capacity). Hence in the following, we use changes in $\overline{\mathrm{pCO_2}}$ and changes in seawater carbonate chemistry synonymously, overall resulting in an enhanced response of $\delta \mathrm{pCO_2}$ to seasonal changes in DIC, TA, T and S.

Considering regional differences, we note that the amplification increases as we move poleward in spite of decreasing $\Delta\overline{\mathrm{pCO_2}}$ (see Fig. 1 and 2). This characteristic geographical pattern of stronger high latitude amplification is the result of larger present-day sensitivities ($\gamma_{\mathrm{DIC_s}}$, γ_{T}) and seasonal amplitudes (δDIC_s, δT) in the high latitudes that amplify the effect of $\Delta\overline{\mathrm{pCO_2}}$ even when its value is small compared to other regions (see Eq. (4), first row term). Some exceptions can be found south of Greenland and near the subtropical gyres, where $\Delta\overline{\mathrm{pCO_2}}$ reaches higher values and therefore they also present large amplification. We also found spatial differences on smaller scales; for example, the western Equatorial Pacific presents lower initial δpCO_2 and amplification than the eastern Equatorial Pacific (see Fig. 1). This is because the eastern side of the basin has larger DIC_s and T contributions than the western side (see Supplementary Fig. S2), as consequence of the upwelling of cold, CO_2-rich waters in the east, which lower the buffering capacity and induce larger δpCO_2 amplitude due the seasonal effects of productivity and solubility (Valsala et al., 2014).

To further disentangle which of the two main drivers (DIC_s or T) is most affected by $\Delta\overline{\mathrm{pCO_2}}$, we decomposed the DIC_s and T

contributions in their sensitivity, seasonal cycle and $\overline{\mathrm{pCO_2}}$ components. Figure 6, (b), shows the total DIC and T components together with the $\Delta\overline{\mathrm{pCO_2}}$ and seasonal cycles effects on them. The effects from the sensitivities are not depicted, as they only play a minor role. Only the $\Delta\gamma_{\mathrm{DIC}}$ term gains importance in the Southern Ocean (not shown). In most of the ocean, the $\Delta\overline{\mathrm{pCO_2}}$ effect on T contribution is the leading cause of amplification. This effect is the result of seasonal solubility changes acting over a larger [CO_2] (Gorgues et al., 2010). In the northern high latitudes, an increase on δT reinforces the amplification. In general, the $\Delta\delta\mathrm{T}$ contribution gains importance as we move poleward in both hemispheres and therefore the second order terms originating from $\Delta\overline{\mathrm{pCO_2}} \cdot \Delta\delta\mathrm{T}$ also reinforce the amplification. Interestingly, in the high latitudes, the amplification through second order terms is as important as the change in the seasonality of the drivers.

The Southern Ocean is an exception to the T dominance; in this region the $\Delta\overline{\mathrm{pCO_2}}$ effect on the $\mathrm{DIC_s}$ contribution dominates, and the regional amplification is reinforced by low values of the mean buffering capacity (high $\gamma_{\mathrm{DIC_s}}$). This result agrees with the findings of Hauck and Völker (2015). In this area the amplification is counteracted by a reduction in $\delta\mathrm{DIC_s}$.

4 Conclusions

In this study, we used output from 7 CMIP5 global models, subjected to the RCP8.5 radiative forcing scenarios, to provide a comprehensive analysis of the characteristics and drivers of the intensification of the seasonal cycle of pCO_2 between present (2006-2026) and future (2080-2100) conditions. By 2080-2100 the δpCO_2 will be 1.5-3 times larger compared to 2006-2026. The projected amplification by the earth-system models and the possible causes of it, are consistent with observation-based amplification for the period from 1982 to 2015 (Landschützer et al., 2018). However, the models slightly overestimate the present day amplification, probably due the larger pCO_2 trends in models than observations (Tjiputra et al., 2014).

The models confirm the well-established mechanisms controlling present-day δpCO_2 (Takahashi et al., 2002; Sarmiento and Gruber, 2006; Fay and McKinley, 2017). $\mathrm{DIC_s}$ and T contributions are the main counteracting terms dominating the seasonal evolution of δpCO_2. Furthermore, the models show that under future conditions the controlling mechanisms remain unchanged. This result confirms the findings of Landschützer et al. (2018) that identified the same regional controlling mechanism for the past 30 years. The relative role of the DIC and T terms is regionally dependent. High latitudes and upwelling regions, such as the California Current system and the coast of Chile, are dominated by $\mathrm{DIC_s}$ and the temperate low latitudes are driven by T. Only in the North Atlantic and North-Western Pacific the models show a dominance of thermal effects over non-thermal effects, which is in disagreement with observations. This further illustrates the urgent need for models to accurately represent regional oceanographic features to accurately reproduce the δpCO_2 characteristics.

In agreement with Landschützer et al. (2018), also the model projections towards the end of this century demonstrate that the global amplification of δpCO_2 is due to the overall longterm increase of anthropogenic CO_2. A higher oceanic background CO_2 concentration enhances the effect of T-driven solubility changes on δpCO_2 and alters the seawater carbonate chemistry, also enhancing the DIC seasonality effect. The spatial differences of δpCO_2 amplification, however, are determined by the regional sensitivities and seasonality of pCO_2 drivers. For example, polar regions show larger sensitivity to DIC and T and larger seasonal cycles of DIC and T. Therefore, these areas present a strong enhancement of δpCO_2, in spite of smaller changes

in mean pCO_2.

Moreover, the pCO_2 seasonal cycle amplitude depends on the relative magnitude and phase of the contributions. The models ensemble mean reproduces the highly effective compensation of DIC_s and T contributions when they are six months out of phase, confirming previous studies (Takahashi et al., 2002; Landschützer et al., 2018). The compensation of DIC and T prevents a larger amplification of δpCO_2, even when both contributions are largely amplified.

The amplification of the TA and S contributions have a small impact on δpCO_2 in most regions, except in the high latitudes where the TA contribution complements the DIC one, enhancing the non-thermal effect in this region.

The use of earth system models allowed us to state the importance of including future changes on the drivers' seasonalities for future δpCO_2 projections. The T seasonality is projected to increase in most of the ocean basins, thereby reinforcing the δpCO_2 amplification. The δT increase is consistent with an increase in stratification that will confine the seasonal changes in net heat fluxes to a shallower mixed layer (Alexander et al., 2018). The DIC_s seasonality decreases in some cold areas and its reduction prevents a larger amplification. For the sensitivities, while γ_{DIC} increases, γ_T decreases. The later phenomenon needs further study.

The increasing amplitude of δpCO_2 might have implications for the net air-sea flux of CO_2, in particular in regions where there is an imbalance between winter and summer values (Gorgues et al., 2010). Examples of such behavior can be found in the Southern Ocean (between 50°S-60°S) (Takahashi et al., 2014a) and in the latitude band from 20°-40° in both hemispheres (Landschützer et al., 2014). Moreover, seasonal events of high pCO_2 could have an impact on acidification and aragonite undersaturation events (Sasse et al., 2015) and hypercapnia conditions (McNeil and Sasse, 2016). Therefore, understanding the drivers of future δpCO_2 may help to better assess the response of marine ecosystems to future changes in carbonate chemistry. Finally, our complete analytical expansion of δpCO_2 in terms of all its 4 variables provides a practical tool to accurately and quickly diagnose temperature and salinity sensitivities from observational or modelling datasets.

5 Acknowledgements

This work was supported by the National Science Foundation under Grant No. 1314209 and by the Institute for Basic Science (IBS), South Korea under IBS-R028-D1. We thank Peter Landschützer for kindly providing his data-sets of thermal and non-thermal components of the pCO_2 seasonal cycle.

References

Alexander, M. A., Scott, J. D., Friedland, K. D., Mills, K. E., Nye, J., Pershing, A. J., and Thomas, A. C.: Projected sea surface temperatures over the 21st century: Changes in the mean, variability and extremes for large marine ecosystem regions of Northern Oceans, Elem. Sci. Anth., 6, 9, 2018.

Bopp, L., Resplandy, L., Orr, J. C., Doney, S. C., Dunne, J. P., Gehlen, M., Halloran, P., Heinze, C., Ilyina, T., Safarian, R., Tjiputra, J., and Vichi, M.: Multiple stressors of ocean ecosystems in the 21st century: projections with CMIP5 models, Biogeosciences, 10, 6225–6245, 2013.

Carton, J. A., Ding, Y., and Arrigo, K. R.: The seasonal cycle of the Arctic Ocean under climate change, Geophys. Res. Lett., 42, 7681–7686, 2015.

Egleston, E. S., Sabine, C. L., and Morel, F. M. M.: Revelle revisited: Buffer factors that quantify the response of ocean chemistry to changes in DIC and alkalinity, Global Biogeochem. Cycles, 24, GB1002, 2010.

Fassbender, A. J., Sabine, C. L., and Palevsky, H. I.: Nonuniform ocean acidification and attenuation of the ocean carbon sink, Geophys. Res. Lett., 44, 8404–8413, 2017.

Fay, A. R. and McKinley, G. A.: Correlations of surface ocean pCO_2 to satellite chlorophyll on monthly to interannual timescales, Global Biogeochem. Cycles, 31, 436–455, 2017.

Gorgues, T., Aumont, O., and Rodgers, K. B.: A mechanistic account of increasing seasonal variations in the rate of ocean uptake of anthropogenic carbon, Biogeosciences, 7, 2581–2589, 2010.

Goris, N., Tjiputra, J., Olsen, A., Schwinger, J., Lauvset, S. K., and Jeansson, E.: Constraining projection-based estimates of the future North Atlantic carbon uptake, Journal of Climate, 31(10), 3959–3978, 2018.

Hagens, M. and Middelburg, J. J.: Attributing seasonal pH variability in surface ocean waters to governing factors, Geophys. Res. Lett., 43, 12,528–12,537, 2016.

Hauck, J. and Völker, C.: Rising atmospheric CO_2 leads to large impact of biology on Southern Ocean CO_2 uptake via changes of the Revelle factor, Geophys. Res. Lett., 42, 1459–1464, 2015.

Hauri, C., Friedrich, T., and Timmermann, A.: Abrupt onset and prolongation of aragonite undersaturation events in the Southern Ocean, Nat. Clim. Change, 6, 172–176, 2015.

IPCC: IPCC Climate Change 2013: The Physical Science Basis. Contribution of Working Group I to the Fifth Assessment Report of the Intergovernmental Panel on Climate Change, 2013.

Kwiatkowski, L. and Orr, J.: Diverging seasonal extremes for ocean acidification during the twenty-first century, Nat. Clim. Change, 8, 141–145, 2018.

Landschützer, P., Gruber, N., Bakker, D. C. E., and Schuster, U.: Recent variability of the global ocean carbon sink, Global Biogeochem. Cycles, 28, 927–949, 2014.

Landschützer, P., Gruber, N., and Bakker, D.: An updated observation-based global monthly gridded sea surface pCO_2 and air-sea CO_2 flux product from 1982 through 2015 and its monthly climatology (NCEI Accession 0160558). Version 2.2. NOAA National Centers for Environmental Information. Dataset. doi:10.7289/V5Z899N6, 2017.

Landschützer, P., Gruber, N., Bakker, D. C. E., Stemmler, I., and Six, K. D.: Strengthening seasonal marine CO_2 variations due to increasing atmospheric CO_2, Nat. Clim. Change, 8, 146–150, 2018.

Lovenduski, N. S., Gruber, N., Doney, S. C., and Lima, I. D.: Enhanced CO_2 outgassing in the Southern Ocean from a positive phase of the Southern Annular Mode, Global Biogeochem. Cycles, 21, GB2026, 2007.

Mckinley, G. A., Takahashi, T., Buitenhuis, E., Chai, F., Christian, J. R., Doney, S. C., Jiang, M., Lindsay, K., Moore, J. K., Quere, C. L., Lima, I., Murtugudde, R., Shi, L., and Wetzel, P.: North Pacific carbon cycle response to climate variability on seasonal to decadal timescales, J. Geophys. Res., 111, C07S06, 2006.

McNeil, B. I. and Sasse, T. P.: Future ocean hypercapnia driven by anthropogenic amplification of the natural CO_2 cycle, Nature, 529, 383–386, 2016.

Pilcher, D. J., Brody, S. R., Johnson, L., and Bronselaer, B.: Assessing the abilities of CMIP5 models to represent the seasonal cycle of surface ocean pCO_2, J. Geophys. Res. Oceans, 120, 4625–4637, 2015.

Sabine, C. L., Feely, R. A., Gruber, N., Key, R. M., Lee, K., Bullister, J. L., Wanninkhof, R., Wong, C., Wallace, D. W. R., Tilbrook, B., Millero, F. J., Peng, T. H., Kozyr, A., Ono, T., and Rios, A. F.: The oceanic sink for anthropogenic CO_2, Science, 305, 367–371, 2004.

Sarmiento, J. L. and Gruber, N.: Ocean Biogeochemical Dynamics, Princeton University Press, Princeton, New Jersey, USA, 2006.

Sasse, T., McNeil, B. I., Matear, R., and Lenton, A.: Quantifying the influence of CO_2 seasonality on future aragonite undersaturation onset, Biogeosciences, 12, 6017–6031, 2015.

Shaw, E. C., McNeil, B. I., Tilbrook, B., Matear, R., and Bates, M. L.: Anthropogenic changes to seawater buffer capacity combined with natural reef metabolism induce extreme future coral reef CO_2 conditions, Glob. Change Biol., 19, 1632–1641, 2013.

Steinacher, M., Joos, F., Froelicher, T. L., Bopp, L., Cadule, P., Cocco, V., Doney, S. C., Gehlen, M., Lindsay, K., Moore, J. K., Schneider, B., and Segschneider, J.: Projected 21st century decrease in marine productivity: a multi-model analysis, Biogeosciences, 7, 979–1005, 2010.

Takahashi, T., Olafsson, J., Goddard, J. G., Chipman, D. W., and Sutherland, S. C.: Seasonal variation of CO_2 and nutrients in the high-latitude surface oceans: A comparative study, Global Biogeochem. Cycles, 7, 843–878, 1993.

Takahashi, T., Sutherland, S. C., Sweeney, C., Poisson, A., Metzl, N., Tilbrook, B., Bates, N., Wanninkhof, R., Feely, R. A., Sabine, C. L., Olafsson, J., and Nojiri, Y.: Global sea-air CO_2 flux based on climatological surface ocean pCO_2, and seasonal biological and temperature effects, Deep-Sea Research II, 49, 1601–1623, 2002.

Takahashi, T., Sutherland, S. C., Chipman, D. W., Goddard, J. G., Cheng, H., Newberger, T., Sweeney, C., and Munro, D. R.: Climatological distributions of pH, pCO_2, total CO_2, alkalinity, and $CaCO_3$ saturation in the global surface ocean, and temporal changes at selected locations, Mar. Chem., 164, 95–125, 2014a.

Takahashi, T., Sutherland, S. C., Chipman, D. W., Goddard, J. G., Newberger, T., and Sweeney, C.: Climatological Distributions of pH, pCO_2, Total CO_2, Alkalinity, and $CaCO_3$ Saturation in the Global Surface Ocean. ORNL/CDIAC-160, NDP-094. Carbon Dioxide Information Analysis Center, https://doi.org/10.3334/CDIAC/OTG.NDP094, 2014b.

Tjiputra, J. F., Olsen, A. R. E., Bopp, L., Lenton, A., Pfeil, B., Roy, T., Segschneider, J., Totterdell, I. A. N., and Heinze, C.: Long-term surface pCO_2 trends from observations and models, Tellus B, 66, 23 083, 2014.

Valsala, V. K., Roxy, M. K., Ashok, K., and Murtugudde, R.: Spatiotemporal characteristics of seasonal to multidecadal variability of pCO_2 and air-sea CO_2 fluxes in the equatorial Pacific Ocean, J. Geophys. Res. Oceans, 119, 8987–9012, 2014.

Völker, C., Wallace, D. W. R., and Wolf-Gladrow, D. A.: On the role of heat fluxes in the uptake of anthropogenic carbon in the North Atlantic, Global Biogeochem. Cycles, 16(4), 1138, 2002.

Zeebe, R. E. and Wolf-Gladrow, D.: CO_2 in Seawater: Equilibrium, Kinetics, Isotopes, Elsevier Science, Amsterdam, Netherlands, and Philadelphia, PA, USA, 2001.

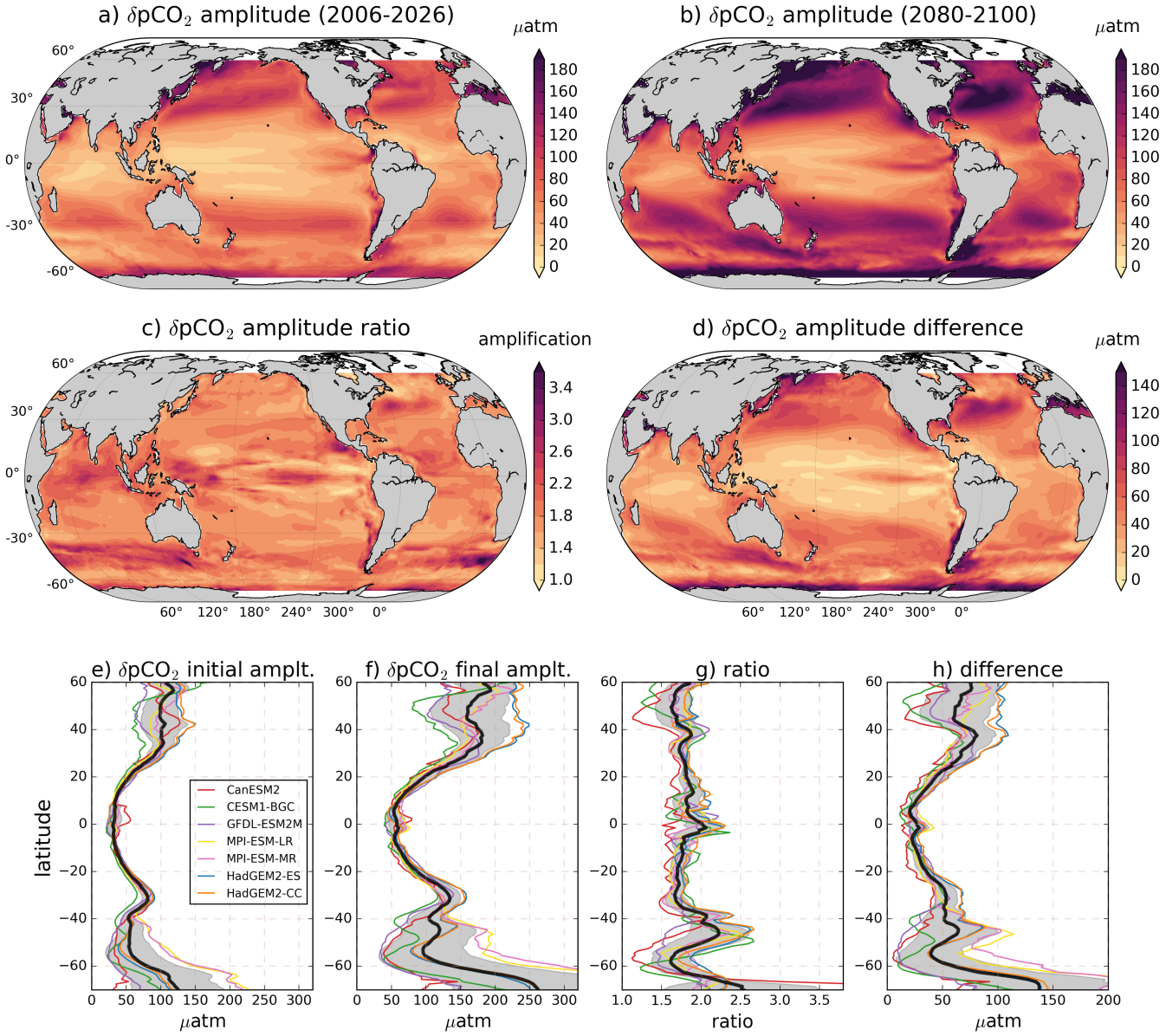

Figure 1. RCP8.5 ensemble mean pCO_2 seasonal cycle amplitude. Amplitude is calculated as climatology maximum-minus-minimum; for a) initial (2006-2026) and b) final (2080-2100) periods. Initial and final climatologies were calculated as the monthly deviation from the respective 21 years period mean. c) and d) show the ratio and difference between the δpCO_2 amplitudes for 2080-2100 and 2006-2026 respectively. e) - h) show the zonal mean of a)- d) respectively, with the individual models shown as colored lines and the ensemble mean overlaid in black. Gray shading represents one standard deviation across the models.

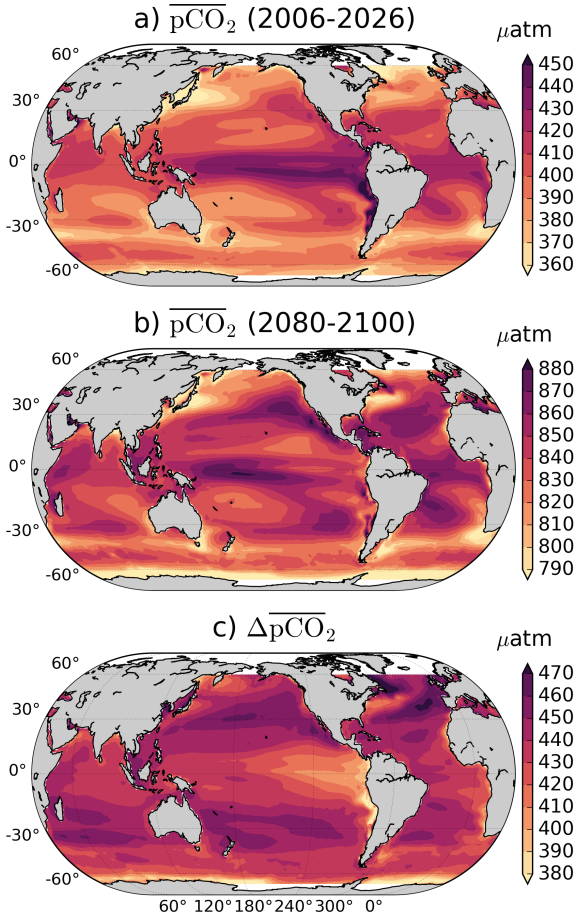

Figure 2. RCP8.5 ensemble mean $\overline{\mathrm{pCO_2}}$: by a) 2006-2026 and b) 2080-2100. c) Difference between 2080-2100 and 2006-2026. The North Atlantic and subpolar gyres, show the largest difference between initial and final periods. The scale is different in each plot to enhance regional features.

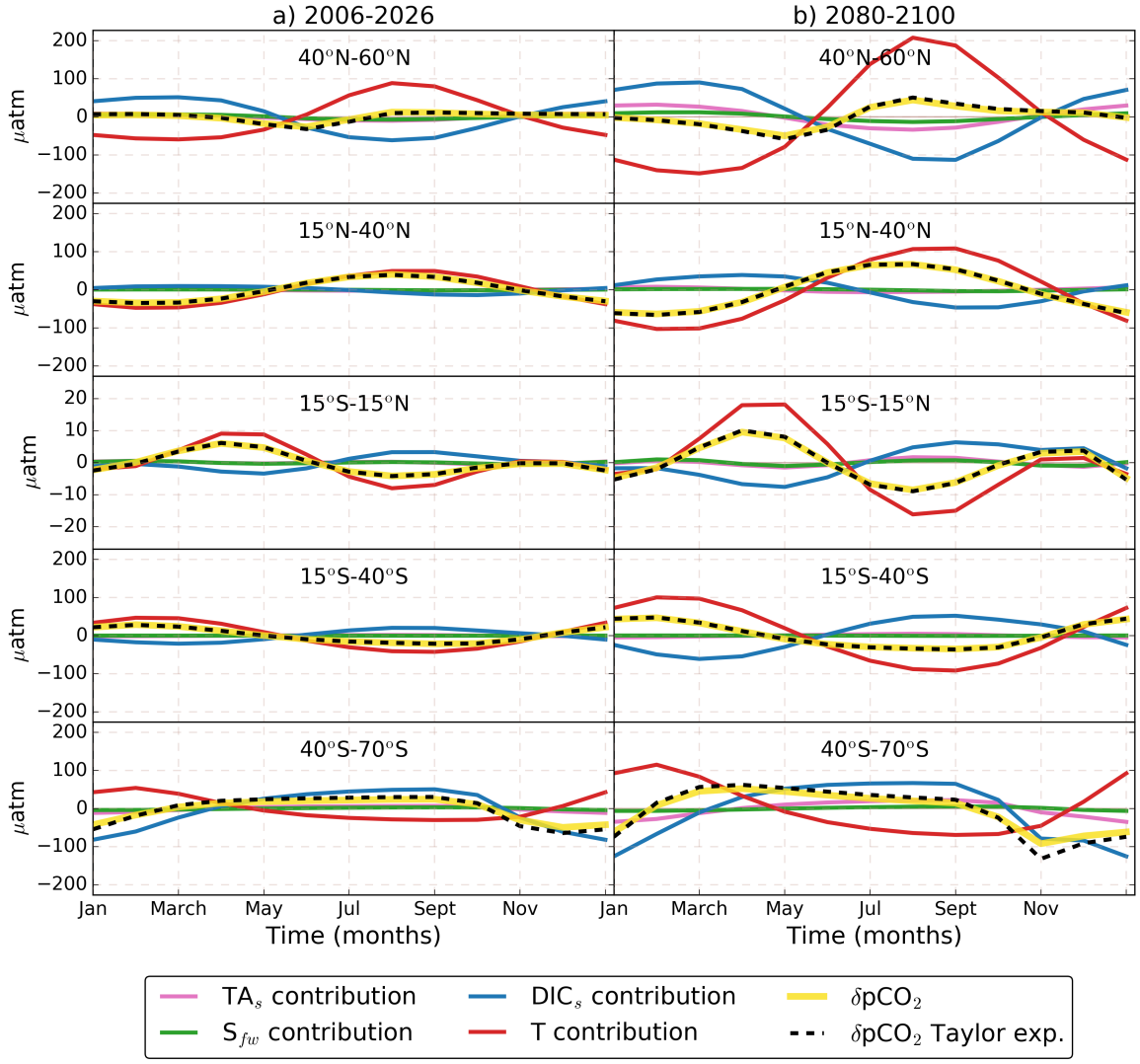

Figure 3. RCP8.5 ensemble mean seasonal cycle (δpCO_2) and its Taylor decomposition. Colored lines indicate the contributions of DIC_s (blue), TA_s (pink), T (red) and S_{fw} (green) to δpCO_2 reconstructed from its Taylor decomposition (Eq. 1) (dashed black). δpCO_2 calculated from monthly pCO_2 (solid yellow) is shown for comparison with the Taylor expansion. Column (a) shows the period 2006-2026 and column (b) shows the period 2080-2100. Each row represents the global zonal average for a different latitudinal band. Temperature dominates all latitudes except the Southern Ocean. In the 40°-60°N band, T contribution is largely compensated by DIC. The TA_s and S_{fw} effects are rather small in all latitudes.

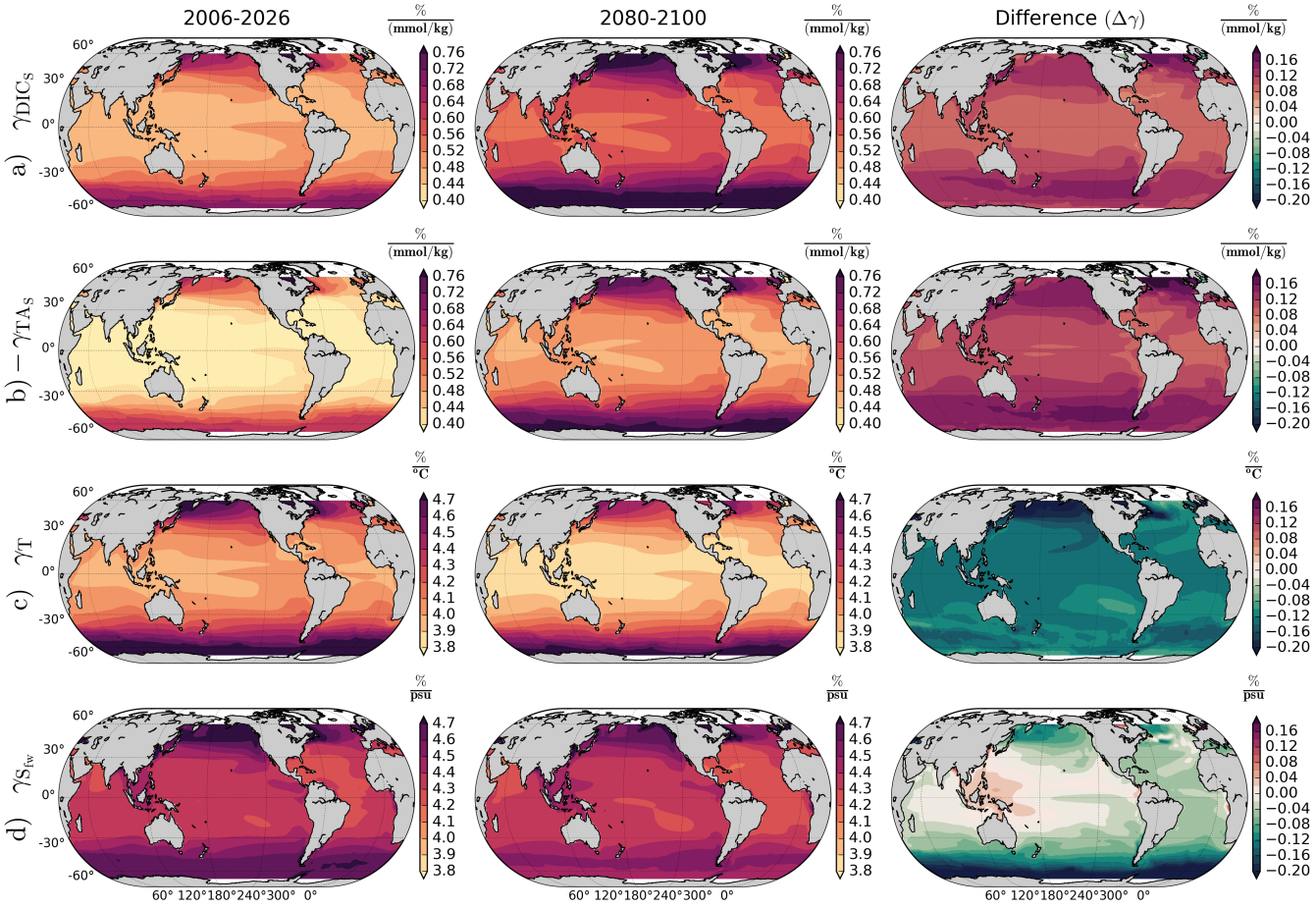

Figure 4. RCP8.5 ensemble mean pCO_2 sensitivities: for DIC_s (row a), TA_s (row b), T (row c) and S_{fw} (row d). Row b) shows the negative of γ_{TA}. The first and second columns show the sensitivities by 2006-2026 and 2080-2100 respectively. The third column shows the difference between 2080-2100 and 2006-2026 sensitivities. High latitudes show the largest difference between initial and final periods. While DIC_s and TA_s sensitivities increase, the T and S_fw sensitivities decreases, except in the Western Pacific Warm Pool, where $\gamma_{S_{fw}}$ increases.

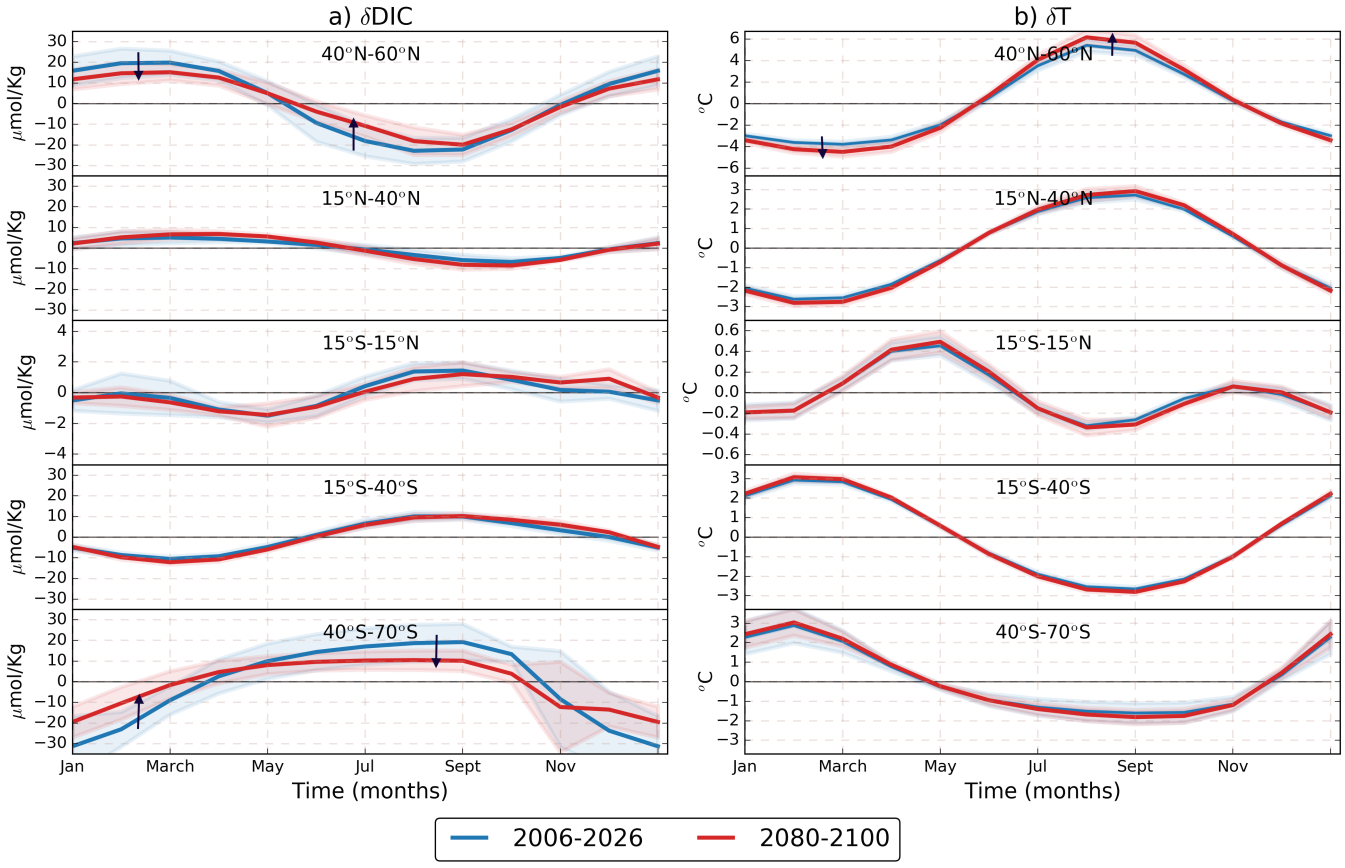

Figure 5. RCP8.5 ensemble zonal mean seasonal cycles: a) δDIC_s and b) δT, for different latitudinal bands. Blue lines represent the 2006-2026 period, depicted for comparison with the 2080-2100 period shown by red lines. Different panels represent different latitudinal sections. Black arrows point out that while T seasonal cycle is projected to increase in most of the ocean, global DIC_s is projected to decrease. The shading represents one standard deviation across the models. It is important to note that the scale is different for some of the latitudinal bands.

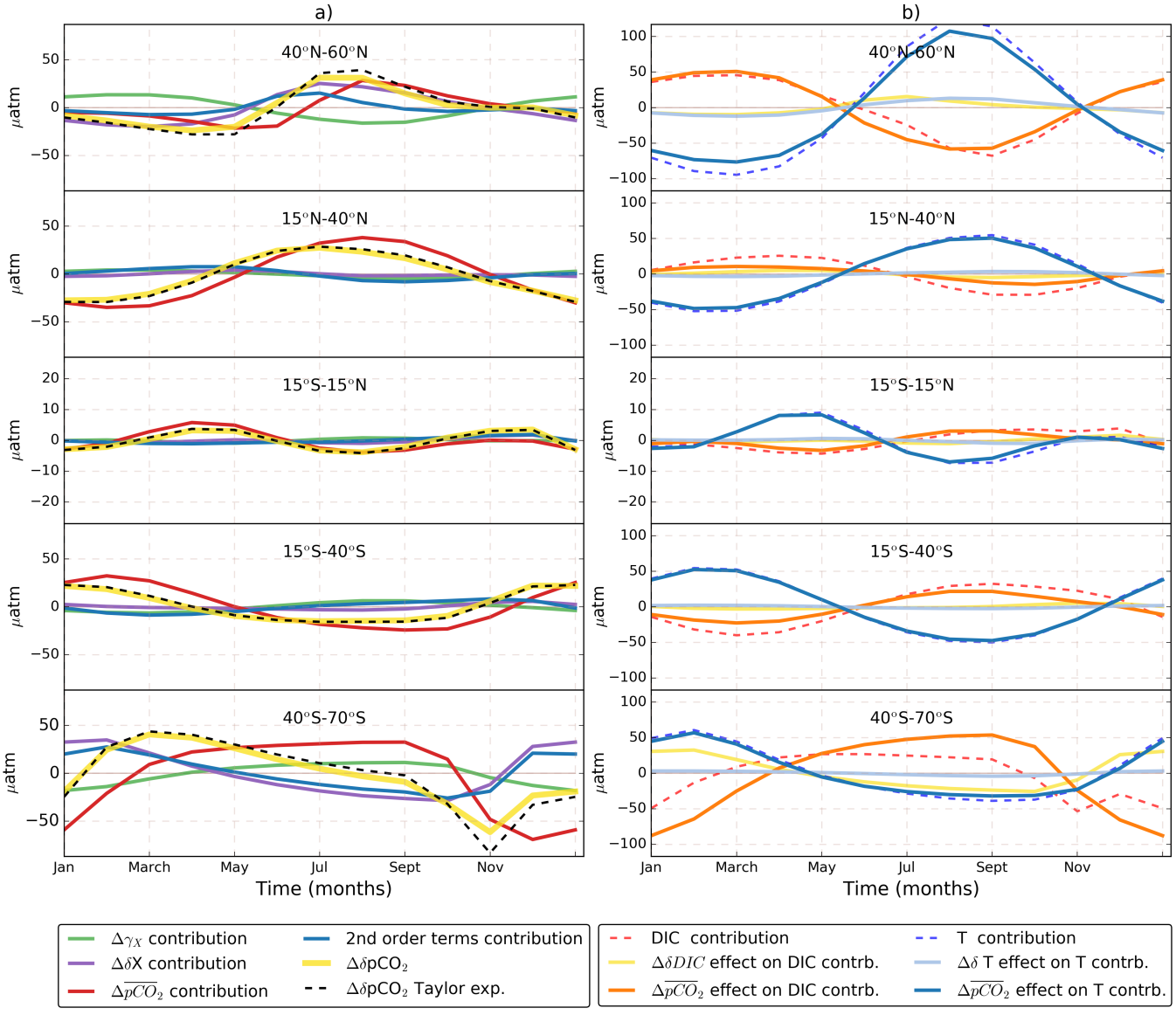

Figure 6. Contribution of seasonalities, sensitivities, and mean pCO_2 changes to $\Delta\delta pCO_2$. a) Time series for the terms of Eq.(4) for different latitudinal bands. The Δ symbol represents the total century change, calculated as 2080-2100 value -minus- 2006-2026 value. The total change in seasonal pCO_2 ($\Delta\delta pCO_2$) is depicted as dashed black. This change is decomposed into changes in seasonalities ($\Delta\delta \boldsymbol{X}$, purple), sensitivities ($\Delta\gamma_X$, green), mean pCO_2 ($\Delta\overline{pCO_2}$, red) and second order terms (blue) summed over the four variables that control pCO_2 (DIC, TA, T and S). For comparison with the expansion, $\Delta\delta pCO_2$ is calculated from model output (yellow). Column b) shows the total change of DIC (dashed red) and T (dashed blue) contributions. Also shown, are two components of the total change on these contributions; the $\Delta\overline{pCO_2}$ effect on the DIC (solid orange) and T (solid blue) contributions, and the $\Delta\delta$DIC (yellow) and $\Delta\delta$T (light blue) effects. In column a), the δpCO_2 change follows the $\Delta\overline{pCO_2}$ effect. Column b) shows that actually, the leading cause of amplification is the $\Delta\overline{pCO_2}$ effect on the T contribution. It is important note the different scale between column a) and b). Also, the scale was reduced in the 15°S-15°N region to highlight its features.